as VC^+, VCH^+, and VCH_2^+ which are not seen with zinc. Similar reactivity is observed for reactions of vanadium ions with other alkanes.[27] Conversely, reaction 2 is not observed for the reaction of vanadium ions with ethane and propane. For the isobutane and neopentane systems, this process is observed although it is small relative to the competing VCH_3^+ channel.

There are many dissimilarities between V^+ and Zn^+ which may account for their different reactivity. At first glance, one of the striking differences is that vanadium has a much lower ionization potential (6.74 eV) than zinc (9.458 eV). Considering only the reactant molecular orbitals analogous to those shown in Figure 5, the difference in the orbital energy (IP) of the metal ions does not change the *relative* ordering of the orbitals. Thus, the lower ionization potential of vanadium should not affect the qualitative correlations.

The most important consideration is electronic structure. The ground state of Zn^+ is ^2S ($3d^{10}4s^1$) while for V^+ it is ^5D ($3d^4$). If we were to consider only the 4s orbital from the vanadium ion, the orbital correlations would be the same as in the zinc system. Mixing of the filled σ_{RM} and the now empty 4s of V^+ would occur. The *diabatic* path would still be the formation of R^+, for both the vanadium and the zinc system, in this simplistic MO approach. But the d orbitals must be considered in the vanadium case, and this complicates the molecular correlation picture. Depending on the symmetry, some of the d orbitals will remain unperturbed and nonbonding, while others will be involved in avoided crossings in the MO correlation diagram. The adiabatic pathway will involve many more crossings for the vanadium system compared with zinc.

The reactions of vanadium ions with various hydrocarbons have been interpreted based on the assumption that the reaction proceeds by metal-ion insertion into C–C or C–H bonds.[26] Formation of such an intermediate complex would be facilitated by the availability of empty d orbitals and would allow electronic reorganization to occur. This is consistent with the dominance of the adiabatic processes in the reactions of V^+ with alkanes. Similar considerations presumably hold for Sc^+, Ti^+, Fe^+, Co^+, and Ni^+.

Preliminary results for the reactions of two other s^1 ions, Ca^+ ($4s^1$) and Mn^+ ($3d^54s^1$), with ethane have been examined for slow rising threshold behavior and for the presence of reaction 2. Neither is observed in the Ca^+ system. Although not a transition metal, it is possible that the empty d orbitals on Ca^+ contribute to its bonding, much like the vanadium system. For Mn^+, reaction 2 is not observed. Reaction 1 is observed but the existence of a small amount (<0.2%) of a low-lying excited state of Mn^+ in the reactant beam makes the interpretion difficult. The apparent threshold for ground-state Mn^+ is definitely greater than the thermodynamic value, and the position of the peak cross section for reaction 1 is unusually high in energy. These observations are consistent either with slow rising threshold behavior or a barrier to the reaction or both. Preliminary data from reaction 1 for Mn^+ with neopentane are consistent with the slow rising threshold interpretation of the ethane data. Thus while the cross section behavior found in this study for Zn^+ is not completely general, indications are that it is representative of a class of systems.

Acknowledgment. This research is supported by Grant No. CHE-8306511 from the National Science Foundation.

Registry No. C_2H_6, 74-84-0; C_3H_8, 74-98-6; $CH(CH_3)_3$, 75-28-5; $C(CH_3)_4$, 463-82-1; Zn^+, 15176-26-8; Zn, 7440-66-6; CH_3, 2229-07-4; C_2H_5, 2025-56-1; C_3H_7, 2143-61-5; C_4H_9, 2492-36-6; $ZnCH_3$, 42217-98-1; $Zn(CH_3)_2$, 544-97-8.

Laser Spectroscopy of Alkaline Earth Monoalkoxide Free Radicals

C. R. Brazier, L. C. Ellingboe, S. Kinsey-Nielsen, and P. F. Bernath*

Contribution from the Department of Chemistry, University of Arizona, Tucson, Arizona 85721.
Received August 6, 1985

Abstract: We have observed a new class of organometallic free radicals. The reaction of the alkaline earth metals Ca, Sr, and Ba in the vapor phase with the alcohols methanol, ethanol, propanol, and butanol yields the metal monoalkoxides. The species are all locally linear near the metal and exhibit characteristic spin–orbit splittings in the $\tilde{A}^2\Pi$ state. The vibrational frequencies are interpreted and possible reaction mechanisms suggested.

The inteaction of metals with organic molecules is one of the principal themes of modern chemistry. Recently, we have discovered a large number of new gas-phase organometallic free radicals[1] produced by the reaction of Ca, Sr, and Ba vapors with alcohols, aldehydes, ketones, thioethers,[2] isocyanic acid,[3] and carboxylic acids.[4] In this paper we report on the alkaline earth monoalkoxide radicals.

The smallest members of the alkaline earth alkoxide (M–O–R; M = Mg, Ca, Sr, and Ba) series are the triatomic monohydroxides (R = H). The alkaline earth monohydroxide radicals commonly occur in flames containing traces of alkaline earth salts.[5] The flame observations date back to the work of Herschel[6] in 1823, although it was not until 1955 that James and Sugden[7] correctly assigned the carrier of the emission to the alkaline earth monohydroxides. ESR spectra of matrix-isolated BeOH[8] and MgOH[9] suggested that, like the alkali hydroxides, the alkaline earth hydroxides are linear. (Although MgOH has a bent excited state.[10]) More recently infrared spectra of matrix-isolated SrOH and BaOH were observed by Kauffman, Hauge, and Margrave.[11]

(1) Brazier, C. R.; Bernath, P. F.; Kinsey-Nielsen, S.; Ellingboe, L. C. *J. Chem. Phys.* **1985**, *82*, 1043–1045.
(2) Ram, R. S.; Brazier, C. R.; Bernath, P. F., unpublished results.
(3) Ellingboe, L. C.; Bopegedera, A. M. R. P.; Brazier, C. R.; Bernath, P. F. *Chem. Phys. Lett.*, in press.
(4) Brazier, C. R.; Ellingboe, L. C.; Kinsey-Nielsen, S. M.; Bernath, P. F., in preparation.
(5) Alkemade, C. Th. J.; Hollander, Tj.; Snelleman, W.; Zeegers, P. J. Th. *Metal Vapours in Flames*; Pergamon: Oxford, 1982.
(6) Herschel, J. F. W. *Trans. Roy. Soc. Edinburgh* **1823**, *9*, 445–460.
(7) James, C. G.; Sugden, T. M. *Nature (London)* **1955**, *175*, 333–334.
(8) Brom, J. M., Jr.; Weltner, W., Jr. *J. Chem. Phys.* **1976**, *64*, 3894–3895.
(9) Brom, J. M., Jr.; Weltner, W., Jr. *J. Chem. Phys.* **1973**, *58*, 5322–5330.
(10) Harris, D. O., personal communication.
(11) Kauffman, J. M.; Hauge, R. H.; Margrave, J. L. *High Temp. Sci.* **1984**, *18*, 97–118.

0002-7863/86/1508-2126$01.50/0

The key discovery in the alkaline earth alkoxide work was that substantial quantities of cool (500 K) MOH could be produced in a flow reactor (Broida oven[12]) by the reaction of alkaline earth metal vapors with H_2O.[13,14] Rotational analyses of the $\tilde{A}^2\Pi$–$\tilde{X}^2\Sigma^+$ and $\tilde{B}^2\Sigma^+$–$\tilde{X}^2\Sigma^+$ electronic transitions by laser techniques provided bond lengths and vibrational frequencies.[15-20] Wormsbecher and Suenram[21] prepared the next member of the alkoxide series in a Broida oven by the reaction of Ca and Sr metal vapors with CH_3ONO.

During an unsuccessful attempt to make alkaline earth acetylides in a Broida oven, we discovered that acetone reacted with Sr vapor to produce two new free radicals.[1] Further experiments proved that the major product was strontium isopropoxide, $SrOCH(CH_3)_2$. The initial strontium isopropoxide observations encouraged us to explore the gas-phase chemical reactions of alkaline earth metals with alcohols. Our chemical and spectroscopic observations for the reactions of Ca and Sr vapors with methanol, ethanol, 1-propanol, 2-propanol, 1-butanol, 2-butanol, and 2-methyl-2-propanol as well as acetone and acetaldehyde are reported here. Some preliminary work on Ba monoalkoxides is also presented.

Experimental Methods

The alkaline earth monoalkoxides were made in a Broida-type oven[12] by the reaction of a metal vapor (Ca, Sr, or Ba) with a suitable oxidant (alcohol, acetone, or acetaldehyde). The metal was evaporated from a resistively heated alumina crucible and entrained in a flow of argon carrier gas. The argon and metal vapor flowed through a hole (0.6 cm in diameter) in the center of an oxidant ring approximately 6 cm from the crucible. The organic oxidant was added as a vapor through small holes in the oxidant ring to produce a "flame" (there may be no chemiluminescent emission) typically 1 cm wide and 10 cm long. The total pressure was adjusted to about 8 torr by varying the pumping speed and argon flow rate in order to optimize the laser-induced emission signal. The butanols and 2-methyl-2-propanol were heated in order to increase the vapor pressures. The production of metal alkoxide was not a strong function of oxidant partial pressure but, in general, additional oxidant improved the signal.

For our initial strontium plus acetone experiments, it was found that the Sr $^3P_1$–$^1S_0$ atomic line overlapped the molecular transition (cf. Figure 2) and that excitation of the atomic line increased the signal by 3 orders of magnitude. Although the ground-state atoms react at pressures of 8–10 torr, the $^3P_1$ excited atoms produce more product molecules. Thus for most of the experiments two continuous wave dye lasers were used: a single-mode (1-MHz) Coherent 699-29 excited the $^3P_1$–$^1S_0$ atomic transition and a broad band (1-cm^{-1}) Coherent 599-01 excited the molecular transition. The dye lasers were operated with DCM or Pyridine 2 dye and were pumped by Coherent Innova 20 and/or Coherent Innova 90 argon ion lasers. The dye laser output beams (200–1000 mW) were spatially overlapped and focussed into the weakly chemiluminescent metal flames.

Resolved fluorescence detection was accomplished by imaging the laser-induced fluorescence onto the slits of a 0.64-m monochromator equipped with an RCA C31034 photomultiplier and photon-counting detection electronics. The monochromator (not the laser) was scanned to provide a dispersed fluorescence signal. Since the molecular emission was almost entirely relaxed, the laser-induced fluorescence pattern did not depend on the wavelength of the laser. The initial location of the main spectral features was usually established by observation of chemiluminescence produced by a single laser resonant with the atomic line.

Table I. Band Origins of Calcium Monoalkoxides (cm^{-1})

molecule	$\tilde{A}_1{}^2\Pi_{1/2}$	$\tilde{A}_2{}^2\Pi_{3/2}$	$\tilde{B}^2\Sigma^+$
CaOH[a]	15965	16032	18022
$CaOCH_3$	15917	15982	17676
$CaOCH_2CH_3$	15850	15913	
$CaOCH_2CH_2CH_3$	15860	15934	
$CaOCH(CH_3)_2$	15823	15896	
$CaO(CH_2)_3CH_3$	15853	15931	
$CaOCH(CH_3)CH_2CH_3$	15813	15896	
$CaOC(CH_3)_3$	15818	15886	

[a] Reference 14.

Table II. Band Origins of Strontium Monoalkoxides (cm^{-1})

molecule	$\tilde{A}_1{}^2\Pi_{1/2}$	$\tilde{A}_2{}^2\Pi_{3/2}$	$\tilde{B}^2\Sigma^+$
SrOH[a]	14543	14806	16377
$SrOCH_3$	14520	14804	16098
$SrOCH_2CH_3$	14507	14767	16090
$SrOCH_2CH_2CH_3$	14512	14784	16176
$SrOCH(CH_3)_2$	14485	14756	16100
$SrO(CH_2)_3CH_3$	14508	14778	16173
$SrOCH(CH_3)CH_2CH_3$	14472	14745	16098
$SrOC(CH_3)_3$	14480	14749	16041

[a] References 12 and 15.

Table III. Band Origins of Barium Monoalkoxides (cm^{-1})

molecule	$\tilde{A}_1{}^2\Pi_{1/2}$	$\tilde{A}_2{}^2\Pi_{3/2}$	$\tilde{B}^2\Sigma^+$
BaOH[a]	11572	12207	13200
$BaOCH_3$	11448	12108	12923
$BaOCH_2CH_3$	11395	12047	12942
$BaOCH(CH_3)_2$	11363	12003	12922

[a] Reference 16.

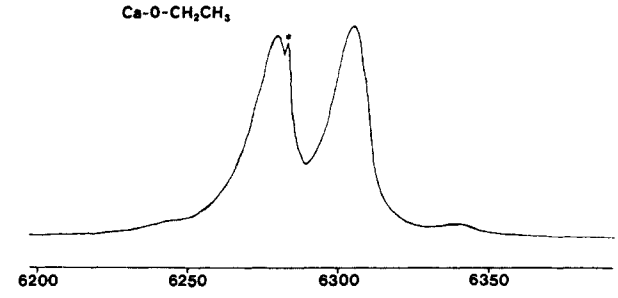

Figure 1. Laser-induced fluorescence from the $\tilde{A}$–$\tilde{X}$ transition of $CaOCH_2CH_3$. The asterisk marks scattered light from the dye laser exciting the $\tilde{A}_2{}^2\Pi_{3/2}$–$\tilde{X}^2\Sigma^+$ molecular transition. The $\tilde{A}_1{}^2\Pi_{1/2}$–$\tilde{X}^2\Sigma^+$ transition is near 6300 Å. An additional laser excited the Ca $^3P_1$–$^1S_0$ transition at 6572 Å. The horizontal scale is in Å.

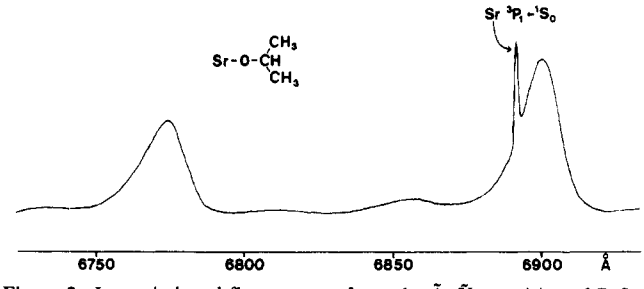

Figure 2. Laser-induced fluorescence from the $\tilde{A}$–$\tilde{X}$ transition of $SrOCH(CH_3)_2$. The laser is simultaneously exciting the atomic line at 6892 Å and the $\tilde{A}_1{}^2\Pi_{1/2}$–$\tilde{X}^2\Sigma^+$ molecular transition. The strong $\tilde{A}_2{}^2\Pi_{3/2}$–$\tilde{X}^2\Sigma^+$ transition is near 6770 Å.

A second laser, resonant with a molecular transition, was then used to provide more intense emission.

Results

The alkaline earth alkoxide spectra all resemble the linear MOH spectra (which, in turn, resemble the MF diatomic spectra) so the observed electronic states will be named by analogy. The two observed electronic transitions are $\tilde{B}^2\Sigma^+$–$\tilde{X}^2\Sigma^+$ and $\tilde{A}^2\Pi$–$\tilde{X}^2\Sigma^+$

(12) West, J. B.; Bradford, R. S.; Eversole, J. D.; Jones, C. R. *Rev. Sci. Instrum.* **1975**, *46*, 164–168.
(13) Benard, D. J.; Slafer, W. D.; Hecht, J. *J. Chem. Phys.* **1977**, *66*, 1012–1016.
(14) Wormsbecher, R. F.; Trkula, M.; Martner, C.; Penn, R. E.; Harris, D. O. *J. Mol. Spectrosc.* **1983**, *97*, 29–36.
(15) Hilborn, R. C.; Qingshi, Z.; Harris, D. O. *J. Mol. Spectrosc.* **1983**, *97*, 73–91.
(16) Nakagawa, J.; Wormsbecher, R. F.; Harris, D. O. *J. Mol. Spectrosc.* **1983**, *97*, 37–64.
(17) Bernath, P. F.; Kinsey-Nielsen, S. M. *Chem. Phys. Lett.* **1984**, *105*, 663–666.
(18) Bernath, P. F.; Brazier, C. R. *Astrophys. J.* **1985**, *228*, 373–376.
(19) Brazier, C. R.; Bernath, P. F. *J. Mol. Spectrosc.* **1985**, *114*, 163–173.
(20) Kinsey-Nielsen, S. M.; Brazier, C. R.; Bernath, P. F. *J. Chem. Phys.* **1986**, *84*, 698–708.
(21) Wormsbecher, R. F.; Suenram, R. D. *J. Mol. Spectrosc.* **1982**, *95*, 391–404.

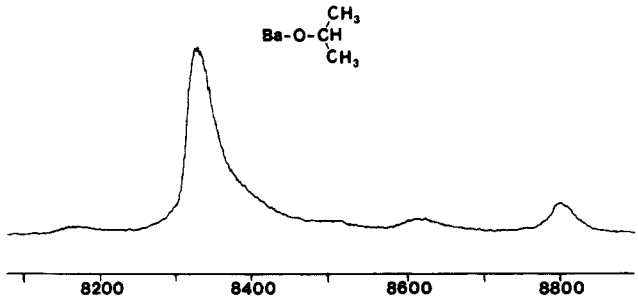

Figure 3. Laser-induced fluorescence from the $\tilde{A}$-$\tilde{X}$ transition of $BaO\text{-}CH(CH_3)_2$. The dye laser excited the $\tilde{B}^2\Sigma^+$–$\tilde{X}^2\Sigma^+$ transition at 7738 Å and the $\tilde{A}$–$\tilde{X}$ transition appears by cascade and relaxed emission. The strong $\tilde{A}_2{}^2\Pi_{3/2}$–$\tilde{X}^2\Sigma^+$ transition lies near 8330 Å, while the equally intense $\tilde{A}_1{}^2\Pi_{1/2}$ component at 8800 Å appears weak because of a sharp decline in photomultiplier tube sensitivity. The horizontal scale is in Å.

with the $\tilde{A}^2\Pi$ state split into two spin components $\tilde{A}^2\Pi_{3/2}$ and $\tilde{A}^2\Pi_{1/2}$ by spin–orbit coupling. Since the symmetry of the alkaline earth alkoxides is lower than linear this is not strictly correct. However, the M–O bond is very ionic so the electronic transitions involve nonbonding M^+ orbitals perturbed by an RO^- ligand. The M–O–C bond angle is 180°. Hence the *local* symmetry near the metal is linear, so for instance, there is always a "spin–orbit" splitting of $\sim$65 cm^{-1} for the $\tilde{A}$ state of the calcium-containing species. The orbitals on the metal are only slightly affected by the nature of R on the ligand, so it is useful to utilize the effective linear symmetry in labeling the electronic states. A more complete description of the electronic structure is presented in the Discussion section.

The observed band origins for calcium, strontium, and barium alkoxides obtained from resolved fluorescence scans are reported in Tables I–III, respectively. Figures 1–3 are typical examples of data recorded by monochromator scans of the laser-induced fluorescence. The hydroxides and methoxides produced resonance fluorescence while emission from the larger molecules was relaxed. The two strong, broad ($\sim$40 cm^{-1}) features of Figures 1–3 are the $\tilde{A}_1{}^2\Pi_{1/2}$–$\tilde{X}^2\Sigma^+$ and $\tilde{A}_2{}^2\Pi_{3/2}$–$\tilde{X}^2\Sigma^+$ transitions. Vibrational relaxation, relaxation between $\tilde{A}_1$ and $\tilde{A}_2$ spin components, and relaxation between $\tilde{B}$ and $\tilde{A}$ states were all prominent (but not complete) in the spectra. The peak positions were determined to an estimated accuracy of ±2–5 cm^{-1}.

The reactions with acetone and acetaldehyde produced strong features identical with those observed with 2-propanol and ethanol, respectively. Formaldehyde did not appear to react, while vinyl alcohol (CH_2=$CHCH_2OH$) and propargyl alcohol (HC≡CCH_2OH) seemed to produce only oxides (CaO, SrO).

The $\tilde{A}$–$\tilde{X}$ emission spectra (Figures 1–3) show evidence of weak vibrational structure. Examples are features near 6250 and 6340 Å in Figure 1, near 6810 and 6860 Å in Figure 2, and 8160 and 8620 Å in Figure 3. The peak near 8800 Å in Figure 3 is a strong $\tilde{A}^2\Pi_{1/2}$–$\tilde{X}^2\Sigma^+$ 0–0 band feature that only appears weak because of rapidly decreasing photomultiplier sensitivity. Since the electronic transition involves a metal-centered, nonbonding electron, the Franck–Condon factors for $\Delta v \neq 0$ transitions are expected to be small. Furthermore, any observed vibrational activity will be associated with the metal center.

In some spectra the detector amplifier gain was such that the strong features were off scale but the vibrational structure was clearer (e.g., Figures 4 and 5). In these two scans the zero of the wavenumber scale is the (off-scale) 0–0 band of the $\tilde{A}^2\Pi_{1/2}$–$\tilde{X}^2\Sigma^+$ transition of CaOR. The structure to the right (to higher wavenumber, to the red in wavelength) represents emission from $v = 0$ of the $\tilde{A}$ state to excited vibrational levels of the $\tilde{X}^2\Sigma^+$ state. The observed transitions could be assigned to activity in four normal modes: ν_B, the M–O–R bend; ν_S, the M–O strength; ν_σ, the O–C stretch; and ν_β, the O–C–C bend. The vibrational frequencies are listed in Tables IV–VI. The accuracy of the vibrational data is ±3 cm^{-1} at best and is worse (±10–20 cm^{-1}) for blended and weak features. Details of the vibrational assignments are presented in the Discussion section.

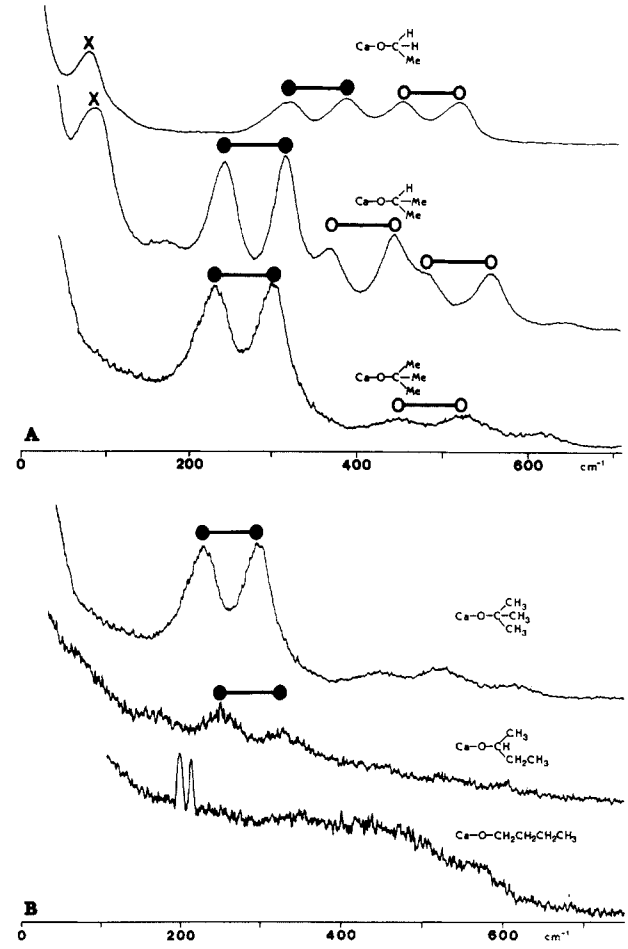

Figure 4. (A) Laser-induced fluorescence spectra of the $CaOCH_2CH_3$, $CaOCH(CH_3)_2$, and $CaOC(CH_3)_3$ molecules (the 0–0 $\tilde{A}$–$\tilde{X}$ band emission is off scale). Each vibrational feature is doubled by the spin–orbit splitting ($\sim$65 cm^{-1}) of the $\tilde{A}$ state. The x-axis scale is set to zero for the $\tilde{A}_1{}^2\Pi_{1/2}$–$\tilde{X}^2\Sigma^+$ 0–0 band so the scale refers to the higher frequency component of any doublet. Each pair of features corresponds to emission from $v = 0$ of the $\tilde{A}$ state into the vibrationally excited levels of the $\tilde{X}^2\Sigma^+$ state. The symbol X marks ν_B, the M–O–R bend, the filled circles are ν_S, the M–O stretch; and the open circles mark the O–C–C bends (ν_β). Pairs of spin–orbit components are connected by horizontal lines. (B) Laser-induced fluorescence spectra of the butoxide isomers $CaOC(CH_3)_3$, $CaOCH(CH_3)CH_2CH_3$, and $CaO(CH_2)_3CH_3$. The bottom two traces are on the same vertical scale while the top trace is a factor of 3 less sensitive. The two sharp features on the bottom trace are artifacts, probably from CaOH.

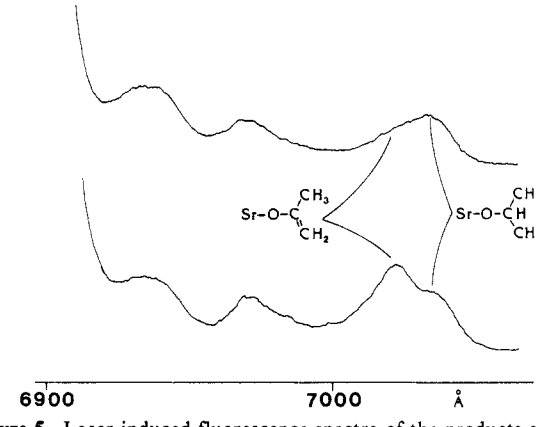

Figure 5. Laser-induced fluorescence spectra of the products of the Sr vapor plus acetone reaction. The $\tilde{A}_1{}^2\Pi_{1/2}$–$\tilde{X}^2\Sigma^+$ transition is off scale near 6903 Å. The upper trace corresponds to a large amount (several hundred millitorr) of acetone oxidant, while the bottom trace was recorded from a flame with less than 100 mtorr of acetone. The vibrational features arise from emission from $v = 0$ of the $\tilde{A}_1{}^2\Pi_{1/2}$ state into vibrationally excited levels of the ground $\tilde{X}^2\Sigma^+$ state (as in Figure 4).

Table IV. Vibrational Frequencies of Calcium Monoalkoxides (cm^{-1})

mode	$\tilde{X}^2\Sigma^+$	$\tilde{A}_1{}^2\Pi_{1/2}$	$\tilde{A}_2{}^2\Pi_{3/2}$	$\tilde{B}^2\Sigma^+$
		$CaOCH_3$		
ν_B	142			166
$2\nu_B$	284			331
ν_S	484	487	486	488
$\nu_B + \nu_S$	625			
$2\nu_S$	973			
ν_σ	1156	1133	1135	
		$CaOCH_2CH_3$		
ν_B	85		95	
ν_S	385	402	400	
ν_B	512	531	533	
mode	$\tilde{X}^2\Sigma^+$	$\tilde{A}_1{}^2\Pi_{1/2}$	$\tilde{A}_2{}^2\Pi_{3/2}$	
		$CaO(CH_2)_3CH_3$		
ν_S		~377		
		$CaOCH(CH_3)CH_2CH_3$		
ν_S	330	339	340	
		$CaOC(CH_3)_3$		
ν_S	302	315	314	
ν_B	520	530	528	
		$CaOCHCH_2CH_3$		
ν_B	74			
ν_S	~349	375	365	
ν_β	~425		~440	
	~578		~557	
		$CaOCH(CH_3)_2$		
ν_B	92		96	
ν_S	319	322	319	
$\nu_{\beta 1}$	440	440	441	
$\nu_{\beta 2}$	551	557	554	
	1013			
ν_σ	1176			

Vibrational structure was difficult to detect for some of the heavier alkoxides. For the alkoxides the intensity of the main peaks of the $\tilde{A}$–$\tilde{X}$ emission (Tables I–III) decreased in approximate proportion to the vapor pressure of the parent alcohol. However, the vibrational features in the spectra decreased in intensity much more rapidly for any molecule containing a chain of three or more carbon atoms (Figure 4). For example, the vapor pressure of 2-butanol is about a factor of 2 less than 2-methyl-2-propanol at room temperature, yet the Ca–O stretch (the pair of peaks near 300 cm^{-1} in Figure 4) has decreased a factor of 20 in intensity.

The reaction of Sr with acetone (and acetaldehyde) produced two products. For instance (Figure 5) when a large (several hundred millitorr) amount of acetone was present, the main product was $SrOCH(CH_3)_2$. At lower acetone concentrations an additional molecule, tentatively assigned to $SrOC(CH_3)=CH_2$, was observed. The strontium isopropoxide assignment is secure since a comparison spectrum (obtained from Sr plus 2-propanol) is available. The reaction of Ca with acetone (or acetaldehyde) produced almost entirely the isopropoxide (ethoxide) while the corresponding Ba reactions have not been explored yet.

Discussion

Chemistry. The direct reaction

$$M + HOR \rightarrow MOR + H$$

is probably endothermic for ground-state Ca and Sr atoms and slightly exothermic for Ba. The RO–H bond energies[22] are in the range 102–106 kcal/mol (except for H–OH, where D_H = 119 kcal/mol). The bond energies of M–OR are, however, known only for Mg–OH (74 kcal/mol),[23] Ca–OH (92 kcal/mol),[24] Sr–OH (92 kcal/mol),[24] and Ba–OH (107 kcal/mol).[24] Since the bonding is ionic and very similar for all of the molecules, we assume that the bond energies are approximately the same for all M–OR. The direct reaction is thus too endothermic to be the main route for MOR production from ground-state Ca and Sr atoms.

If the alkaline earth atoms are excited by laser irradiation on the $^3P_1$–$^1S_0$ atomic transition the direct reaction becomes exothermic. For Ca, Sr, and Ba the lowest $^3P_1$ states provide 44, 41, and 36 kcal/mol, respectively, of additional energy to the reaction.[25] Thus, the 3 orders of magnitude enhancement in product molecule concentration observed with M* reagents is probably due to the direct reaction channel becoming available. Excited Ca* and Sr* (Ba* was not tested) atoms react 3 orders of magnitude more readily than ground-state Ca and Sr.

The gas-phase reaction of ground-state Ca, Sr, and Ba atoms with H_2O and alcohols is unexpected and remarkable. Two

Table V. Vibrational Frequencies of Strontium Monoalkoxides (cm^{-1})

mode	$\tilde{X}^2\Sigma^+$	$\tilde{A}_1{}^2\Pi_{1/2}$	$\tilde{A}_2{}^2\Pi_{3/2}$
		$SrOCH_3$	
ν_S	408	423	430
$2\nu_S$	806		
ν_σ	1141		
		$SrOCH_2CH_3$	
ν_B	78	81	83
ν_S	345		357
	434		
ν_β?	490		496
ν_σ	1154		
		$SrOCH_2CH_2CH_3$	
ν_B	65	~70	~70
ν_S	279		274
ν_β?	368		320
	550		542
		$SrOCH(CH_3)_2$	
ν_B	78	93	91
ν_S	274		291
$\nu_{\beta 1}$	421	409	419
$\nu_{\beta 2}$	533		539
		$SrO(CH_2)_3CH_3$	
ν_B	~53		
ν_S	~265		~295
		$SrOCH(CH_3)CH_2CH_3$	
ν_B	61		
$2\nu_B$	125		
ν_S			~280
		$SrOC(CH_3)_3$	
$2\nu_B$	142		
ν_S	247		261
ν_β	498		497
		$SrOC(CH_3)=CH_2$	
ν_S	253		248
ν_β	510		486
		$SrOCH=CH_2$	
ν_S	306		273

Table VI. Vibrational Frequencies of Barium Monoalkoxides (cm^{-1})

mode	$\tilde{X}^2\Sigma^+$	$\tilde{A}_1{}^2\Pi_{1/2}$	$\tilde{A}_2{}^2\Pi_{3/2}$
		$BaOCH_3$	
$2\nu_B$	254		
ν_S	375	342	344
		$BaOCH_2CH_3$	
ν_S		279	279
		$BaOCH(CH_3)_2$	
ν_S	249	243	247

(22) McMillen, D. R.; Golden, D. M. *Annu. Rev. Phys. Chem.* **1982**, *33*, 493–532.
(23) Murad, E. *Chem. Phys. Lett.* **1980**, *72*, 295–296.
(24) Murad, E. *J. Chem. Phys.* **1981**, *75*, 4080–4085.
(25) Moore, C. E. *Atomic Energy Levels*; National Bureau of Standards: Washington, DC 1971; Vol. I-III, NSRDS-NBS 35.

Table VII. Metal–Oxygen Stretching Frequencies (ν_S) for Alkaline Earth Monoalkoxides (cm^{-1})

molecules	M		
	Ca	Sr	Ba
MOH	606[a]	528[b]	492[c]
$MOCH_3$	486	408	375
$MOCH_2CH_3$	385	345	
$MOCH_2CH_2CH_3$	~349	279	
$MOCH(CH_3)_2$	319	274	249
$MO(CH_2)_3CH_3$		~265	
$MOCH(CH_3)CH_2CH_3$	330		
$MOC(CH_3)_3$	302	247	
$MOCH{=}CH_2$		306	
$MOC(CH_3){=}CH_2$		253	

[a] Reference 11. [b] Reference 15. [c] Reference 16.

possible mechanisms for ground-state Ca, Sr, and Ba atom reactions are

Mechanism A

$$M + H\text{–}OR \xrightarrow{Ar} H\text{–}M\text{–}OR$$
$$H\text{–}M\text{–}OR + M \rightarrow MH + M\text{–}OR$$
$$MH + H\text{–}OR \rightarrow MOR + H_2$$
$$M + H\text{–}OR \rightarrow MOR + {}^1/_2H_2$$

Mechanism B

$$M + H\text{–}OR \xrightarrow{Ar} H\text{–}M\text{–}OR$$
$$H\text{–}M\text{–}OR + H\text{–}OR \rightarrow M(OR)_2 + H_2$$
$$M(OR)_2 + M \rightarrow 2\ MOR$$
$$M + H\text{–}OR \rightarrow MOR + {}^1/_2H_2$$

The first step involves the insertion of the metal atom into the H–O bond. The presence of a third body (Ar carrier gas) increases the probability of this event and accounts for our observation that high pressures (8–10 torr), produced by decreasing the pumping speed, increased the metal monoalkoxide concentration. The HMOR intermediate was not detected because it probably has no visible electronic absorption spectrum. However, Kauffman, Hauge, and Margrave[11] have observed the photolytic insertion of Mg, Ca, Sr, and Ba into H–OH. The HMOH product was trapped in an argon matrix and monitored by infrared absorption spectroscopy.

In mechanism A the second step involves the production of the MH species. The Ca, Sr, and Ba reactions with formic and acetic acids[1] did produce MH. Since MH was not observed in our metal plus alcohol experiments, mechanism B is favored. $M(OR)_2$ should have a UV absorption spectrum and would not be observed in our visible laser experiments.

The above two mechanisms are simply plausible speculations. It is possible that surface reactions in the crucible play a role or (more likely) that metal dimers and clusters are involved. Like the superficially simple Bunsen burner flame, the flame chemistry of a Broida oven system may also be quite complicated.

The reaction of Sr with acetone (or acetaldehyde) is unusual because a reduction of Sr isopropoxide (or ethoxide) dominates the chemistry. The simplest explanation is that a 2-propanol impurity in the acetone is responsible, but it is unlikely that this represents the only route to Sr isopropoxide. A more promising explanation involves the addition of SrH or HSrOR across the carbonyl double bond of acetone. The additional vibrational features that are not Sr isopropoxide (Figure 5) are tentatively assigned to the Sr acetone enolate (Table V) because this is the only other product likely to have a spectrum so similar to that observed for Sr isopropoxide.

Vibrational Structure. The metal-centered character of the $\tilde{A}$–$\tilde{X}$ electronic transition both helps and hinders the vibrational analysis. Franck–Condon selection of only a few modes associated with the metal center makes the vibrational assignments relatively easy.

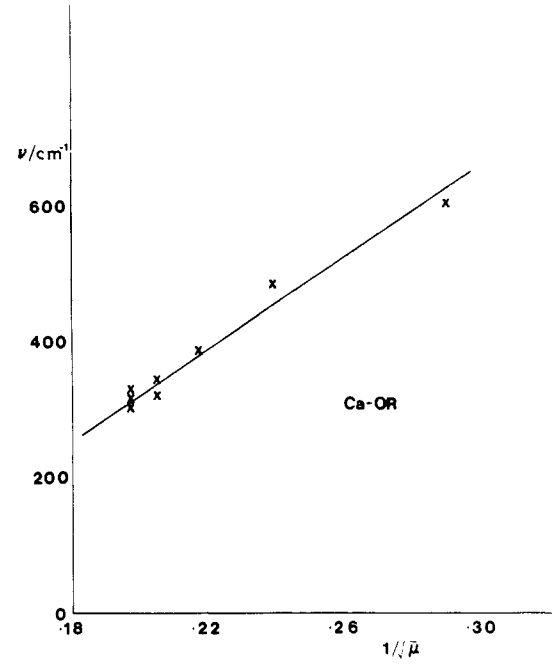

Figure 6. A plot of the Ca–O stretching frequency vs. the inverse square root of the "reduced mass" for the series CaOR (R = H, CH_3, C_2H_5, C_3H_7, C_4H_9).

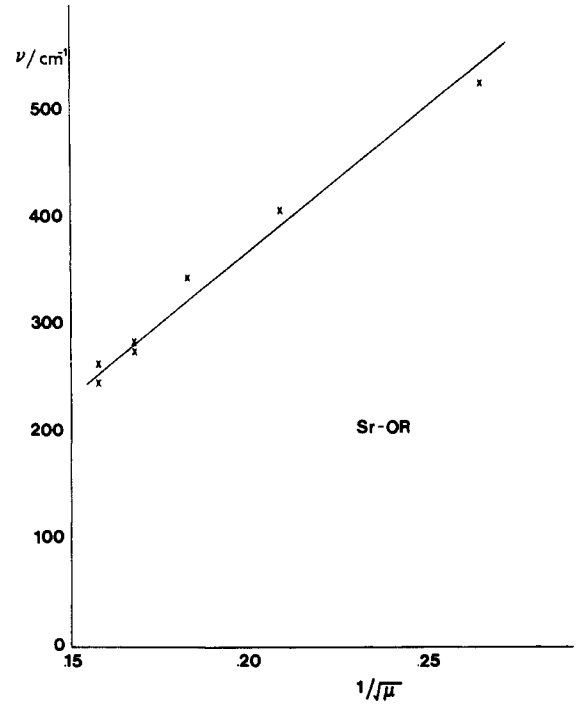

Figure 7. The variation of the Sr–O stretching frequency for the series SrOR (R = H, CH_3, C_2H_5, C_3H_7, C_4H_9).

However, almost all direct information about the nature of the alkyl group is suppressed.

The metal–oxygen stretching frequency (ν_S) is usually the strongest mode (Figure 4, indicated by solid circles) and was easily assigned. The ground-state ν_S frequencies are collected in Table VII for comparison purposes. The values range from 606 cm^{-1} for CaOH to 247 cm^{-1} for $SrOC(CH_3)_3$, largely because of changes in the effective reduced mass. The M^+–O^- ionic bonding results in a similar M–O force constant for all the observed molecules. By treating the OR unit as a single mass a diatomic-like "reduced mass" (μ) can be calculated. A plot of the stretching frequency vs. $\mu^{-1/2}$ produces an approxmately linear correlation with Ca–OR and Sr–OR (Ba has only three points) each producing a slightly different line (Figures 6 and 7).

Many of the solid alkaline earth dialkoxide compounds have been synthesized and characterized by infrared spectroscopy.[26-28] The $M(OR)_2$ molecules form crystalline solids so the infrared spectra below 500 cm^{-1} are dominated by lattice modes.[26-28] Unfortunately, lattice modes cannot be directly correlated with gas-phase M–OR stretches or bends. Our M–OR stretch frequencies are in the range of other metal alkoxide frequencies,[29-31] although the state of aggregation is often unknown for many compounds.

The M–OR bending mode (ν_B) is usually as prominent as the M–O stretching mode. In fact for Sr alkoxides with symmetry lower than C_{3v} ν_B is the strongest mode, occurring in the 65–90-cm^{-1} region except for MOH and $MOCH_3$. This is a remarkably low frequency even for a bending mode but the ionic M^+–O^- bond will produce a very flat bending potential. The low frequency is also consistent with the general trend in bending frequencies for CaOH (339 cm^{-1}) and $CaOCH_3$ (142 cm^{-1}).

The intensity of transitions involving ν_B and $2\nu_B$ is informative and sometimes puzzling. A long progression in ν_B (or any other mode) is not observed so by the Franck–Condon principle there is little change in geometry. Furthermore, since MOH is linear, $MOCH_3$ and $MOC(CH_3)_3$ probably have C_{3v} symmetry while the other molecules have either C_S or no symmetry for all electronic states (although the local symmetry near the metal remains $C_{\infty v}$). For the $C_{\infty v}$ and C_{3v} molecules ν_B has π or e symmetry so only $2\nu_B$ should appear in an electronic transition.[32] Within the Born–Oppenheimer approximation the selection rule for non-totally symmetric vibrations[32] is $\Delta v = \pm 2, \pm 4, \ldots$ However, the 000–010 vibronic transition (involving ν_B) is observed weakly for MOH,[19,20] probably because of spin–orbit vibronic coupling.[19] The ν_B vibration is also observed weakly in $CaOCH_3$ and $SrOCH_3$ but not in $BaOCH_3$, $CaOC(CH_3)_3$, and $SrOC(CH_3)_3$ because the signal-to-noise ratio was not high enough. In the molecules with symmetry lower than C_{3v} the ν_B mode is no longer degenerate and at least one component is not forbidden and often appears quite strongly. For example in Figure 4A ν_B appears (near 90 cm^{-1}, marked by an X) for $CaOCH_2CH_3$ and $CaOCH(CH_3)_2$ but not for $CaOC(CH_3)_3$.

The O–C stretch (ν_σ) occurs weakly near 1150 cm^{-1} for some of the smaller molecules for which the signal-to-noise ratio is high. This frequency is about 100 cm^{-1} higher than the O–C stretch observed in the corresponding alcohols[33-36] or in inorganic complexes such as $Cr(OCH_2CH_3)_3$[29] or $U(OCH_3)_6$.[31] The solid-state alkaline earth $M(OCH_3)_2$ and $M(OCH_2CH_3)_2$ molecules have strong bands at ~1050 and 1150 cm^{-1} but Lutz[27,28] assigns (correctly?) the ~1150-cm^{-1} mode to CH_3 rocking and the 1050-cm^{-1} mode to the O–C stretch. Anionic hyperconjugation[37] is expected to strengthen the O–C bond relative to the corresponding alcohols so our 1150-cm^{-1} assignment for the O–C stretch is reasonable.

Additional vibrational modes were observed in the 400–550-cm^{-1} region and were sometimes quite strong (Figure 4A, marked with open circles). We assign these modes to C–C–O bends (ν_B). For the isopropoxides two such modes were found (Figure 4A), possibly corresponding to symmetric and antisymmetric combinations of the two C–C–O bends. For the *tert*-butoxides the three C–C–O bends will form a doubly degenerate (e) mode (forbidden in an electronic transition) and a totally symmetric (a) mode. The totally symmetric mode involves only carbon–carbon motions and will be weak (Figure 4A) because of unfavorable Franck–Condon factors. The C–C–O deformation occurs at 420 cm^{-1} for ethanol,[34] 462 cm^{-1} for 2-methyl-2-propanol,[36] 462 cm^{-1} for $LiOC(CH_3)_3$,[38] and 370 cm^{-1} for $Cr(OCH_2CH_3)_3$.[29]

There are some puzzling aspects to the intensity of vibrational modes for the heavier alkoxides. The metal–oxygen stretching mode (ν_S) decreases rapidly in intensity (relative to the main 0–0 peak) for the isomeric series $CaOC(CH_3)_3$, $CaOCH(CH_3)CH_2CH_3$, and $CaO(CH_2)_3CH_3$ (Figure 4B). One possibility is that the Franck–Condon factors change in this series, but why this should be so for such a similar group of compounds is not clear. Another possibility is suggested by the appearance of a broad "feature" from 100–600 cm^{-1} to the red of the diagonal band in the $CaO(CH_2)_3CH_3$ scan: perhaps the ground-state M–O stretch is mixing with other modes. The suitable low-frequency (100–300 cm^{-1}) torsion modes are quite different in the various isomeric forms. For instance $CaOC(CH_3)_3$ has three CH_3–C torsions while $CaO(CH_2)_3CH_3$ has two CH_2–CH_2 torsions and one CH_2–CH_3 torsion. (There are also more configurations for $CaO(CH_2)_3CH_3$ than for $CaOC(CH_3)_3$.) If the M–O mode is mixed with torsional modes then, a wide bloblike feature could replace an isolated M–O feature as modes with poorer Franck–Condon factors borrow intensity from the M–O stretch.

Electronic Structure. The alkaline earth monoalkoxide electronic spectra resemble those of the corresponding monohalides. The similarities are particularly strong for the isoelectronic MOH as OH^- is a pseudohalide. Since replacing H by R in MOH is not expected to change the basic character of the electronic states, our discussion of MOR electronic states is carried over from the corresponding MF states.[39-41]

The ground $\tilde{X}^2\Sigma^+$ state of MOR arises almost entirely from the valence $ns\sigma$ orbital of M^+ with a small admixture of $np\sigma$ character. The first excited states[25] for Ca^+, Sr^+, and Ba^+ are the $(n-1)$d states with np states 10 000–15 000 cm^{-1} higher (n = 4, 5, and 6 for Ca, Sr, and Ba, respectively). The O^-–R ligand has effective linear symmetry and produces three molecular orbitals $(n-1)d\sigma$, $(n-1)d\pi$ and $(n-1)d\delta$ from the $(n-1)$d orbital and two molecular orbitals $np\sigma$, $np\pi$ from the np state. The $np\sigma$ and $(n-1)d\sigma$ mix to produce the $\tilde{B}^2\Sigma^+$ state while the $np\pi$ and $(n-1)d\pi$ result in the $\tilde{A}^2\Pi$ state (as well as higher lying $^2\Sigma^+$ and $^2\Pi$ states). The $\tilde{B}^2\Sigma^+$ and $\tilde{A}^2\Pi$ states form a unique perturber pair[42] connected by spin–orbit, rotation–electronic, and vibronic interactions. The $(n-1)d\delta$ orbitals produce a $^2\Delta$ state, which for BaCl[43] has been found to lie lower in energy than the $\tilde{A}^2\Pi$ state. The $^2\Delta$ states are difficult to locate because $^2\Delta$–$^2\Sigma$ transitions are forbidden even for pseudodiatomics like MOR. For the calcium and strontium monoformates, where the local symmetry is C_{2v} rather than $C_{\infty v}$, the $^2\Delta$ state (or more accurately a $^2A_1$ state correlating with a $^2\Delta$ parent state) has been found about 1000 cm^{-1} below the $\tilde{A}$ state.[4]

The spin–orbit coupling constants, A, are 73, 281, and 632 cm^{-1} for the $\tilde{A}^2\Pi$ states of CaF,[44] SrF,[45] and BaF,[46] respectively, while the corresponding monohydroxide values are 66,[15,18] 263,[19] and 635 cm^{-1}.[20] The range of values for the alkoxides CaOR, SrOR,

(26) Grigor'ev, A. I.; Turova, N. Ya. *Dokl. Akad. Nauk SSSR*, **1965**, *162*, 98–101.
(27) Lutz, H. D. *Z. Anorg. Allg. Chem.* **1967**, *353*, 207–215.
(28) Lutz, H. D. *Z. Anorg. Allg. Chem.* **1968**, *356*, 132–139.
(29) Brown, D. A.; Cunningham, D.; Glass, W. K. *J. Chem. Soc. A* **1968**, 1563–1568.
(30) Casey, A. T.; Clark, R. J. H. *Inorg. Chem.* **1969**, *8*, 1216–1222.
(31) Cuellar, E. A.; Miller, S. S.; Marks, T. J.; Weitz, E. *J. Am. Chem. Soc.* **1983**, *105*, 4580–4589.
(32) Herzberg, G. *Electronic Spectra and Electronic Structure of Polyatomic Molecules*; Van Nostrand Reinhold: New York, 1966; pp 150–157.
(33) Shimanouchi, T. *Tables of Molecular Vibrational Frequencies*; National Bureau of Standards: Washington, DC, 1972, Vol. I, NSRDS-NBS 39, p 63.
(34) Perchard, J. P.; Josien, M. L. *J. Chim. Phys. Physico-Chim. Biol.* **1968**, *65*, 1834–1855.
(35) Fukushima, K.; Zwolinski, B. J. *J. Mol. Spectrosc.* **1968**, *26*, 368–383.
(36) Korppi-Tommola, J. *Spectrochim. Acta, Part A* **1978**, *34A*, 1077–1085.
(37) Seubold, F. H., Jr. *J. Org. Chem.* **1956**, *21*, 156–160.
(38) Simonov, A. P.; Shigorin, D. N. *Optics Spectrosc.* **1967**, *Suppl. 3*, 123–125.
(39) Dagdigian, P. J.; Cruse, H. W.; Zare, R. N. *J. Chem. Phys.* **1974**, *60*, 2330–2339.
(40) Bernath, P. F.; Pinchemel, B.; Field, R. W. *J. Chem. Phys.* **1981**, *74*, 5508–5515.
(41) Rice, S. F.; Martin, H.; Field, R. W. *J. Chem. Phys.* **1985**, *74*, 5023–5034.
(42) Zare, R. N.; Schmeltekopf, A. L.; Harrop, W. J.; Albritton, D. L. *J. Mol. Spectrosc.* **1973**, *46*, 37–66.
(43) Martin, H.; Royen, P. *Chem. Phys. Lett.* **1983**, *97*, 127–129.
(44) Bernath, P. F.; Field, R. W. *J. Mol. Spectrosc.* **1980**, *82*, 339–347.
(45) Steimle, T. C.; Domaille, P. J.; Harris, D. O. *J. Mol. Spectrosc.* **1978**, *73*, 441–443.
(46) Barrow, R. F.; Bastin, M. W.; Longborough, B. *Proc. Phys. Soc., London* **1967**, *92*, 518–519.

and BaOR are 63-78, 260-280 and 635-670 cm^{-1}, respectively (Tables I-III). This similarity in spin-orbit constants suggests that the $\tilde{A}$ states (and probably the $\tilde{B}$ and $\tilde{X}$ states) have similar atomic parentage to the fluorides.

The location of the $\tilde{B}$ and $\tilde{A}$ states relative to each other and the $\tilde{X}$ state also suggests close similarity with the MF molecules. The band origins ($v = 0$) for $\tilde{B}^2\Sigma^+$, $\tilde{A}^2\Pi_{3/2}$ and $\tilde{A}^2\Pi_{1/2}$ states are 18833,[47] 16566,[44] and 16493 cm^{-1}; 17271,[48] 15372,[45] and 15091 cm^{-1}; 14040,[46] 12262,[46] and 11630 cm^{-1} for CaF, SrF, and BaF, respectively. In general, the larger the alkyl group the more red shifted are the $\tilde{A}$-$\tilde{X}$ and $\tilde{B}$-$\tilde{X}$ transitions (Tables I-III).

The splitting between the $\tilde{A}$ and $\tilde{B}$ states is a ligand field separation between $d\sigma$ ($p\sigma$) and $d\pi$ ($p\pi$) orbitals. The various ligands can be arranged in a spectrochemical series[49] $F^- > OH^- > NH_2^- > O^-R > NCO^- > Cl^- > Br^- > I^-$ for the alkaline earths. The order is determined by the $\tilde{B}$-$\tilde{A}$ energy separation and reflects the strength of the ligand field interaction. The location of NH_2^- is from the work of Wormsbecher et al.[14] and our $SrNH_2$ observations.[50] Note that $SrNH_2$ has C_{2v} symmetry so that $\tilde{A}^2\Pi$ further splits into $^2B_1$ and $^2B_2$ states. The NCO^- splitting is from our own recent discovery of the CaOCN and SrOCN molecules.[3]

(47) Dulick, M.; Bernath, P. F.; Field, R. W. *Can. J. Phys.* **1980**, *58*, 703-712.
(48) Steimle, T. C.; Domaille, P. J.; Harris, D. O. *J. Mol. Spectrosc.* **1977**, *68*, 134-145.
(49) Cotton, F. A.; Wilkinson, G. *Advanced Inorganic Chemistry*, 4th ed.; Wiley: New York, 1980; p 663.

Conclusion

A large number of new Ca-, Sr-, and Ba-containing free radicals have been discovered and characterized by laser spectroscopy. The alkaline earth monoalkoxides were produced in the gas phase by the reaction of the metal vapor with the appropriate alcohol. The vibrational and electronic structure of the akaline earth monoalkoxides has been explained in terms of an M^+ ion perturbed by an O^-R ligand.

Acknowledgment. This research was supported by the National Science Foundation (NSF-8306504) and the Research Corporation. Acknowledgement is made to the donors of the Petroleum Research Fund, administered by the American Chemical Society, for partial support of this work. Partial support was also provided by the Office of Naval Research (ONR N 00014-84-K-0122).

(50) Brazier, C. R; Bernath, P. F., unpublished results.

The Use of a Stationary Cationic Surfactant as a Selective Matrix in ^{252}Cf-Plasma Desorption Mass Spectrometry

Catherine J. McNeal* and Ronald D. Macfarlane

Contribution from the Department of Chemistry, Texas A&M University, College Station, Texas 77843. *Received July 24, 1985*

Abstract: Mylar films impregnated with a cationic surfactant have been tested as an anion exchange matrix for ^{252}Cf-PDMS studies. The purpose of this matrix was to reduce the intermolecular binding forces and the effects of matrix impurities which hinder desorption-ionization of biopolymers bearing multiple anionic groups. The matrix selectively adsorbed the anionic moiety from aqueous solutions of an inorganic salt and several simple nucleic acid fragments. Significant enhancements in the yields were observed.

In many of the particle induced emission mass spectrometric methods (^{252}Cf-PDMS, SIMS, LDMS, FABMS) ionization-desorption occurs from a solid matrix. The disadvantage of ionizing molecules from the solid phase rather than the liquid or gas phase is the complexity of interactions that may attenuate or quench molecular ion formation. Impurities in the matrix or strong interactions between highly polar species have been identified as probable causes.[1] In FABMS when a liquid matrix is used these problems seem to be less severe. It has been proposed that the solvent used in these studies may modify the strong interactions among solute molecules, making it easier to desorb a molecule from the solute-solvent cluster because the binding energy between molecules is reduced. This suggests that molecular ion yields in the solid phase are attenuated when the energy binding a molecule to its surrounding matrix exceeds the energy that is available in the desorption process.[1] In an effort to reduce the strong interactions between molecules in the solid phase we first reported on the use of Nafion as an ion-containing polymer matrix that could selectively bind large organic cations, effectively reducing the interactions.[2] The selectivity of the sulfonic acid groups of Nafion for binding cations was demonstrated by incorporating only Cs^+ and not I^- when the film was exposed to an aqueous solution of CsI. Molecular ions of large organic cations, including Bleomycin-Cu^{2+} complex, adsorbed onto the film have been produced.

The advantages of Nafion are that it is a relatively low equivalent molecular weight polymer (1100 ew) that can be dissolved in an organic solvent system[3] but which will not redissolve after drying if exposed to aqueous solutions. Thin films of Nafion (<100 μg/cm) can be cast on a foil backing, either by electrospray[4] or spin coating.[5] The films are then used as a substrate to selectively adsorb desired cations from a solution. The films contain a high surface concentration of the adsorbed cations due to the low equivalent molecular weight of the polymer. Typical ion exchange resins are not useful because the particulates produce films too thick for ^{252}Cf fission fragments to penetrate and because the equivalent molecular weight is very high, resulting in a low surface concentration of the ions of interest. Furthermore, these films tend to redissolve when exposed to a solution.

We have sought to develop an anion exchange matrix similar to the Nafion that would reduce the intermolecular binding forces and the effects of matrix impurities which were felt to hinder desorption-ionization in ^{252}Cf-PDMS, particularly in the analysis

(1) Macfarlane, R. D. *Acc. Chem. Res.* **1982**, *15*, 268-275.
(2) Jordan, E. A.; Macfarlane, R. D.; Martin, C. R.; McNeal, C. J. *Int. J. Mass Spectrom. Ion Phys.* **1983**, *53*, 345-348.
(3) Martin, C. R.; Rhoades, T. A.; Ferguson, J. A. *Anal. Chem.* **1982**, *54*, 1639-1641.
(4) McNeal, C. J.; Macfarlane, R. D.; Thurston, E. L. *Anal. Chem.* **1979**, *51*, 2036-2039.
(5) Meyerhofer, D. *J. Appl. Phys.* **1978**, *49*, 3993-3997.

0002-7863/86/1508-2132$01.50/0